The MOCVD growth of erbium antimonide nanocomposite embedded III-V host materials and Characterization for thermoelectrics

Takehiro Onishi[1,2], Tela Favaloro[1], Ali Shakouri[1], Elane Coleman[3], Gary S. Tompa[3], and Nobuhiko P. Kobayashi[1,2]

[1]University of California, Santa Cruz (UCSC), Electrical Engineering Department, Santa Cruz, CA 95064, U.S.A.

[2]Nanostructured Energy Conversion Technology and Research (NECTAR)**,** Advanced Studies Laboratories (ASL), NASA Ames Research Center, Moffett Field, CA 94035, U.S.A.

[3]Structred Materials Industries Inc. [www.structuredmaterials.com], Unit 102/103, 201 Circle Drive North, Piscataway, NJ 08854, U.S.A.

Abstract

The target of this study is: (1) to enhance thermoelectric materials by employing nanocomposites into host materials [1], (2) to demonstrate item (1) by MOCVD, and (3) to develop a monitoring technique of ErSb nanocomposites co-deposited with host materials. (I don't know if I like this structure)

We have conducted ErSb thin film growth and ErSb nanocomposite co-deposition with zinc doped host materials InGa_xSb_1-x and In_1-yAs_ySb by MOCVD on InSb (100) substrate respectively. Through the thin film growth studies, we found that ErSb growth rate on InSb (100) substrate has a strong sensitivity to the growth temperature and Sb/Er precursor flow rate ratio. To study the quality of the ErSb layer grown in the peak growth rate conditions, SEM, EDX, and XRD were employed. The smooth surface was observed on the film by SEM. All expected elements, Er, In, and Sb were detected in the EDX results; and XRD spectra indicated that the grown film contained two single crystal structures. Once we established an ErSb thin film growth recipe, we attempted co-deposition of ErSb nanocomposite with zinc doped host III-V ternary alloy. The purpose of this co-deposition is enhancement of host material's thermoelectrics properties , especially to reduce thermal conductivity introducing nanocomposite as a mid-to-long wave length phonon scattering source. Hereby we successfully demonstrated growth of ErSb nanopillar embedded InGa_xSb_1-x:Zn and ErSb nanoparticles embedded In_1-yAs_ySb:Zn respectively. Along with growth recipe development for co-deposition of ErSb nanocomposite with host mateirals, RAIRS (Reflection Absorption Infra-Red Spectroscopy) was employed to develop ex-situ Er monitoring technique. Detecting In-H stretching mode masked by grown ErSb on the In terminated InSb (100) substrate surface, the smallest increment of 2.3 ML from 7.2 ML to 9.5 ML can be distinguished.

Table of Contents (incomplete a differs from paper)

1. Introduction

In the growing energy demand and the seeking of the carbon free energy sources, technologies harvesting unused and wasted energy are getting strong attention. Thermoelectrics are one of the more environmentally friendly power sources under growing investigation. Thermoelectrics convert heat directly into electric power. Despite the several decades quest to improve thermoelectric materials, the conversion efficiency is still far behind its theoretical limit, which has limited broad implementation of thermoelectrics.

However, recent advances using properties associated with the nanoscale have shown great promise in advancing thermoelectrics to their theoretical limits. Nanostructures are one of the promising technologies of new material development and tuning enabling the drastic enhancement of electrical, optical, and thermal properties of the energy conversion materials. In particular, we focus on nanocomposites embedded in host materials having significantly different physical properties and dimensions.

In this research, we demonstrate co-deposition of erbium monoantimonide (ErSb) nanoparticles or nanocolumns in bulk group III –V (In_1-xGa_xSb and InAs_ySb_1-y) ternary alloys with dopant (Zn) for the carrier tuning. The nano scale composites work to maintain electrical properties and optimize heat transport properties of the host materials working as the efficient mid to long-wavelength phonon scattering source along with randomly replaced groups III or V atoms in the host material crystals and the filter of low energy carriers. The net result appears in lower thermal conductivity than that of the alloy-limit and fairly identical level of Seebeck coefficient and electrical conductivity implying the enhancement of the dimensionless figure of merit ZT. (important so why in the middle, organization problem)

Taking advantage of low-pressure Metal Organic Chemical Vapor Deposition (MOCVD), we have developed the growth recipe of erbium antimonide (ErSb) nanocomposites embedded in the zinc (Zn) doped indium gallium (arsenic) antimonide (InGa(As)Sb) host materials. The size of ErSb nanocomposites, carrier density and alloy composition of the host materials are tuned by the control of the growth temperature; flow rate and duration time of component material precursors supply. (awkward sentence)

The structural analyses focusing on surface morphology, crystallographic properties, chemical composition of the Zn doped InGa(As)Sb host materials, and growth features of ErSb nanocomposites. Techniques such as Scanning Electron Microscopy (SEM), Fourier Transform Infra-Red-absorption (FTIR), Atomic Force Microscopy (AFM), X-Ray Diffraction (XRD), and Transmission Electron Microscopy (TEM) were used to obtain information on the co-deposited ErSb nanocomposites and InGa(As)Sb:Zn film on n-type InSb (100) substrate separated with unintentionally doped (UID) InSb buffer layer .

Combined with the temperature dependency of Seebeck coefficient (thermoelectric power) and electrical conductivity of InSb host material on InSb substrate by MOCVD, thermal conductivity of ErSb:InGa(As)Sb:Zn, the quality of MOCVD-grown ErSb-InGa(As)Sb is comparable to that of MBE grown films. That suggests the ZT enhanced [1] nanocomposites embedded thermoelectrics host materials will be possible to produce in the large scale and at high growth rate by MOCVD [1] . (good to know but akward presentation of information)

2. Experiments

(this section feels incomplete or like the flow is off we should talk through the flow—love all the figure through out the paper very effective)

The standard guideline of good thermoelectrics material search is to seek narrow-gap Eg semiconductors with high mobility (m_e and m_h) [2]. The targets of this study is: (1) to enhance thermoelectrics materials employing nanocomposites into host materials [1] , (2) to demonstrate item (1) by MOCVD, and (3) to develop a monitoring technique of ErSb nanocomposites co-deposited with host materials.

2.1 The growth of InSb host material on InSb(100) substrate and characterization

To demonstrate MOCVD thermoelectrics material growth with nanocomposites in dissimilar host materials, we begun with InSb thin film deposition on InSb(100) substrate and measured thermoelectric properties.

Structure Materials Industry (SMI) Inc. pulse MOCVD system (Figure 1) was used in the growth of InSb host material, ErSb thin film; grains, and ErSb nanocomposites co-deposited with ternary host materials. The reactor quartz tube (Figure 2) has vertical impinging precursor supply lines at top for host materials (In: Trimethylindium and Sb: Triethylantimony) and a sub line for nanocomposites (Er: Tri(isopropylcylopentadienyl)Erbium) respectively. The precursors are carried by high grade purified hydrogen gas from the bubbler in the gas system to the substrate horizontally clumped to the susceptor hold at the middle of the tube. The bonding between metal and organic branch in the raw materials are thermally decomposed at 485 °C with assist of plasma then the metallic elements deposit on the substrate surface creating epitaxial layers.

Similar procedures were applied to the growth of ErSb thin film and grains on InSb(100) substrate and UID InSb buffer layer prepared on InSb(100) substrate. Organization problem

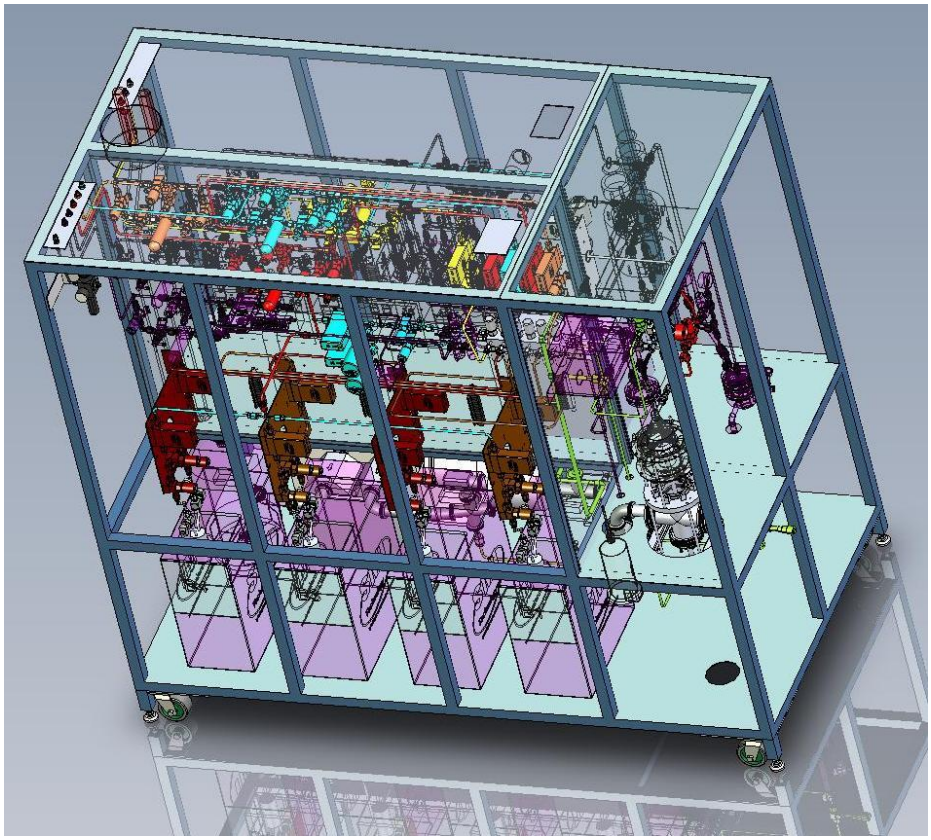

Figure 1 - Structured Materials Industry's pulsed MOCVD system. Four precursor handling systems are in the front reactor stays on the stage in the right front end the system.

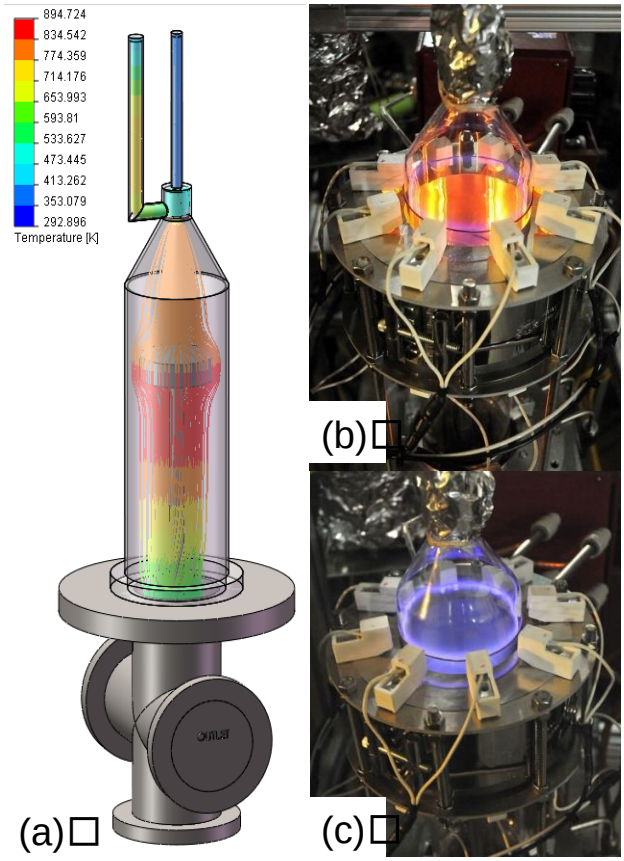

Figure 2 - (a) Schematics of quartz reactor tube and precursor flow with temperature distribution, (b) demonstration of chemical vapor deposition (CVD), (c) grow light of assisting plasma.

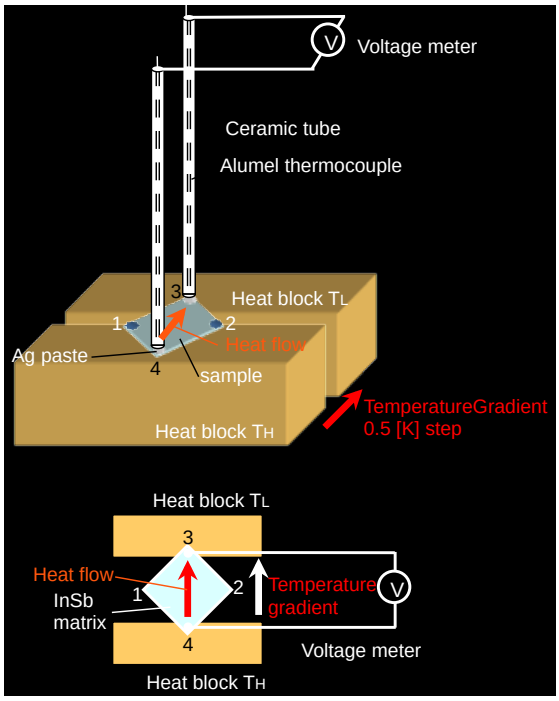

Figure 3- Seebeck coefficient(thermoelectric power) measurement configuration. The sample chip was bridged between two heat blocks. The entire configuration was set in vacuum chamber during the measurement. The vacuum level was about 7.5 E-6 Torr. The temperature of the system was controlled at four temperature levels. After ten minutes to being stable at set temperature, temperature gradient with 5 K step were induced between two end of the sample. At each temperature gradient, 100 times electric potential data acquisitions were conducted. Then the average over 100 data points were plotted as the thermoelectric power of the sample at specific temperature with temperature gradient induced (Figure 2).

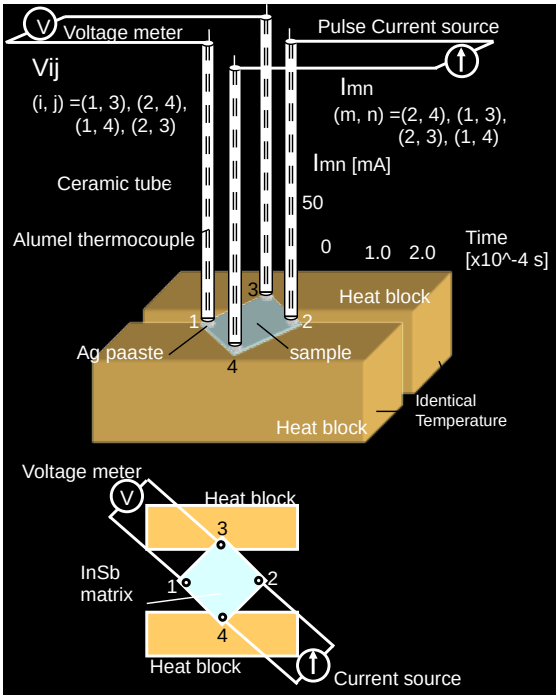

Figure 4 - van der Pauw (electric resistivity) measurement configuration. The same temperature control, induced temperature gradient and data acquisition were conducted as well as Seebeck coefficient measurement with additional two probing points. Obeying regular van der Pauw procedure, resistivity of sample was calculated [3].

2.3 Er monitoring technique development by Reflection Absorption IR Spectroscopy (RAIRS)

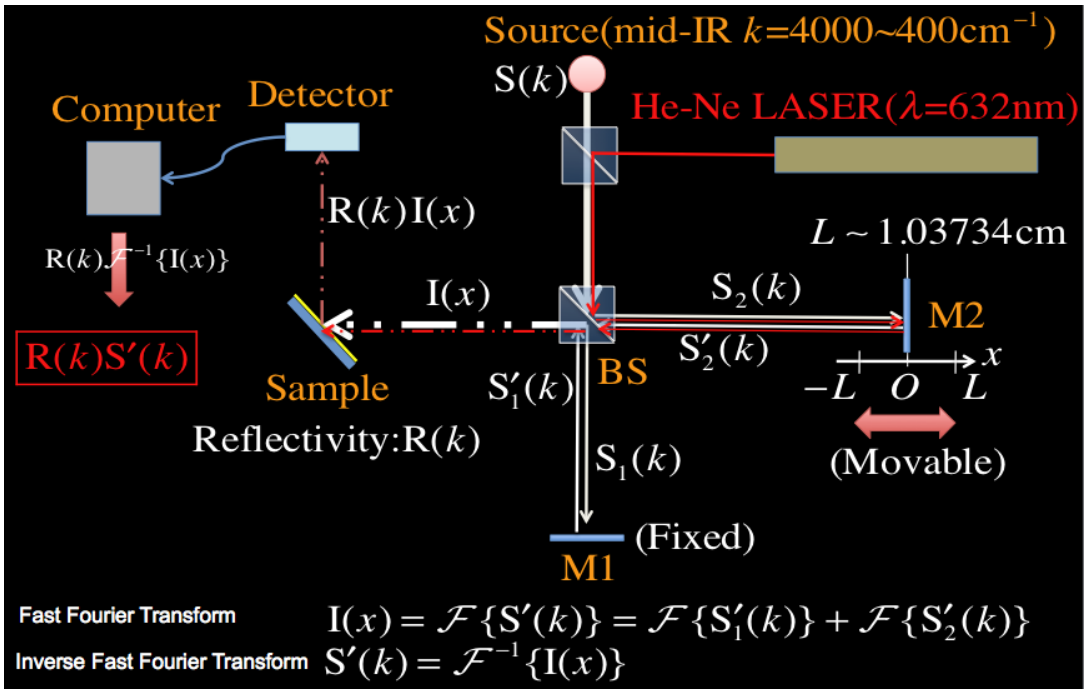

Figure 5 – Fourier Transform Infra-Red (FTIR) spectroscopy configuration.

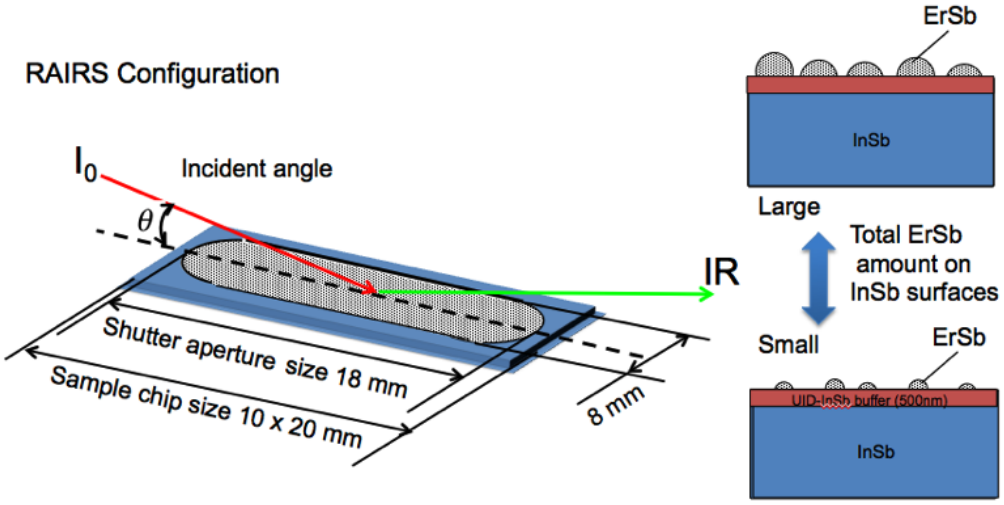

Figure 6 - Reflection absorption infra-red spectroscopy (RAIRS) configuration and expected ErSb cover growth features on 500 nm thickness unintentionally doped InSb buffer layer prepared on n-type InSb (100) substrate.

2.3 Electro Capacitance Voltage of Zn doped host material

In order to calibrate dopant Zn, Electro Chemical Voltage (ECV) measurement was conducted on multilayer test structure in Figure . The structure had four 200 nm test layers with various Zn dose, (12.2 E+7, 6.12 E+7, 3.04 E+7, and 1.21 E+7 cm^-3 from top to bottom) being separated by 50 nm UID InSb layers. The entire test structure was grown on 200 nm UID InSb prepared on n type InSb(100) substrate (Figure). Then carried density of each layers was measured with the configuration in Figure .

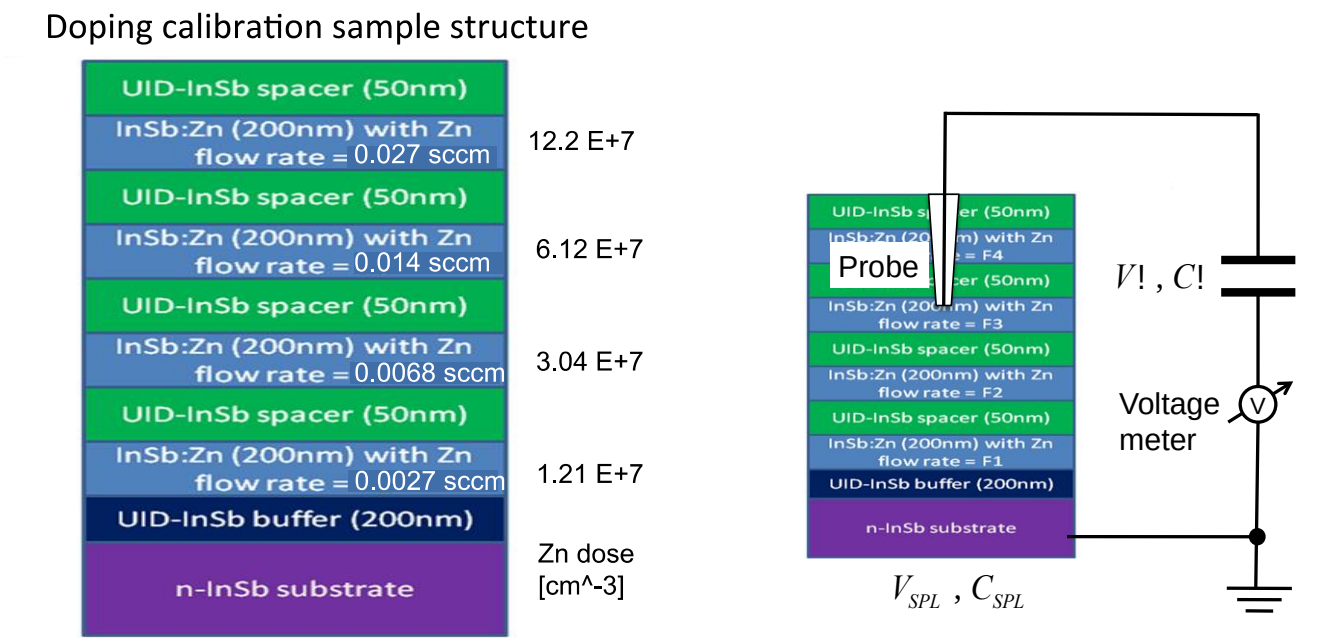

Figure 7 – Electro Chemical Voltage (ECV) multilayer samples for Zn dose calibration. From top to bottom layers, Zn precursor flow rate varied 0.027, 0.014, 0.0068; 0.0027 sccm and target Zn dose amount 12.2 E+7, 6.12 E+7, 3.04 E+7; 1.21 E+7 cm^-3).

2.4 TEM imaging of ErSb nanocomposites co-deposited with host materials

The TEM sample lamellas were processed by Ga2+ iron beam FIB acceleration voltage at 30 kV using vertical curving technique. (1) The processed area is covered by Pt barrier layer, (2) 4 um depth vertical trenches are created in the both side of the lamella, (3) The underneath cut and the left and right slits are created, (4) The both surface of the lamella are polished by the iron beam into 50 ~ 60 nm thickness (Figure 7), (5) The lamella is scraped off and transferred by tipped glass capillary micro-manipulator onto a copper TEM grid.
Then TEM images were taken with electron acceleration voltage at 200 kV and z direction of electron beam [110].

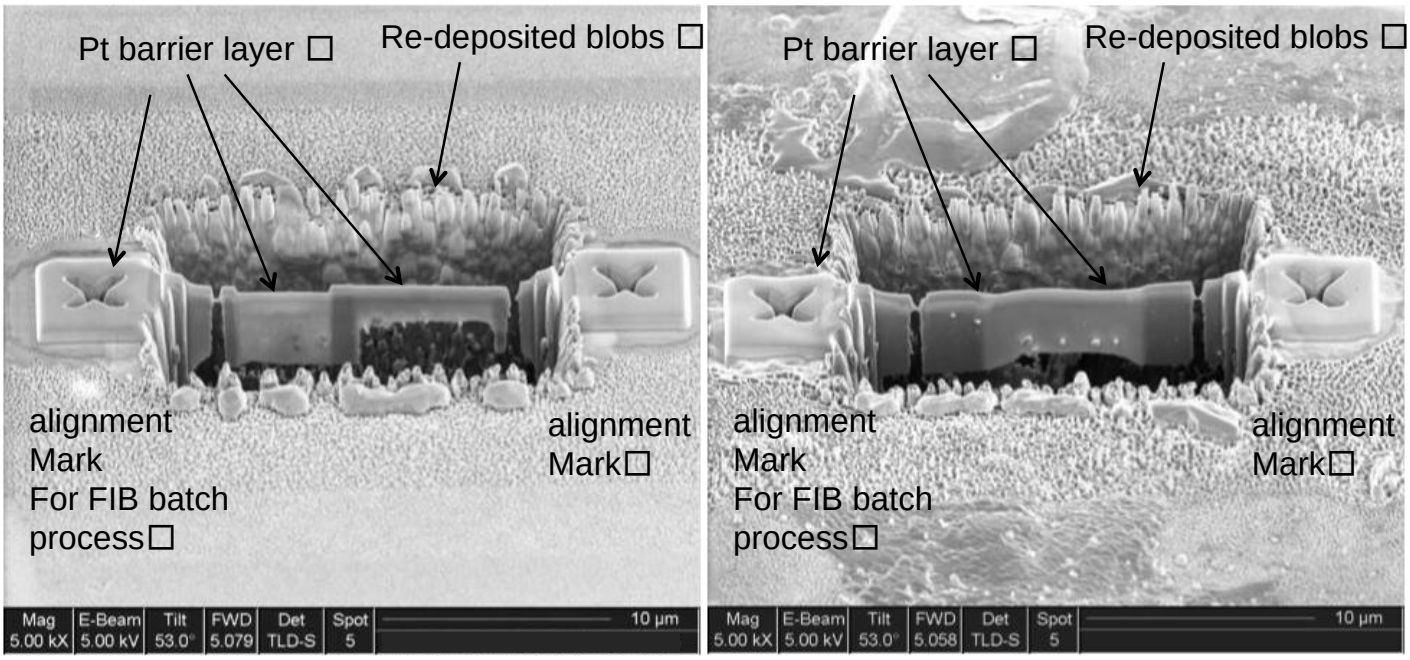

Figure 8 – TEM sample lamellas processed by Ga ion FIB with vertical curving technique. (left) ErSb co-deposited with InGa_xSb_1-x:Zn film (X=0.975), and (right) ErSb co-deposited In_1-yAs_ySb:Zn (Y=0.406).

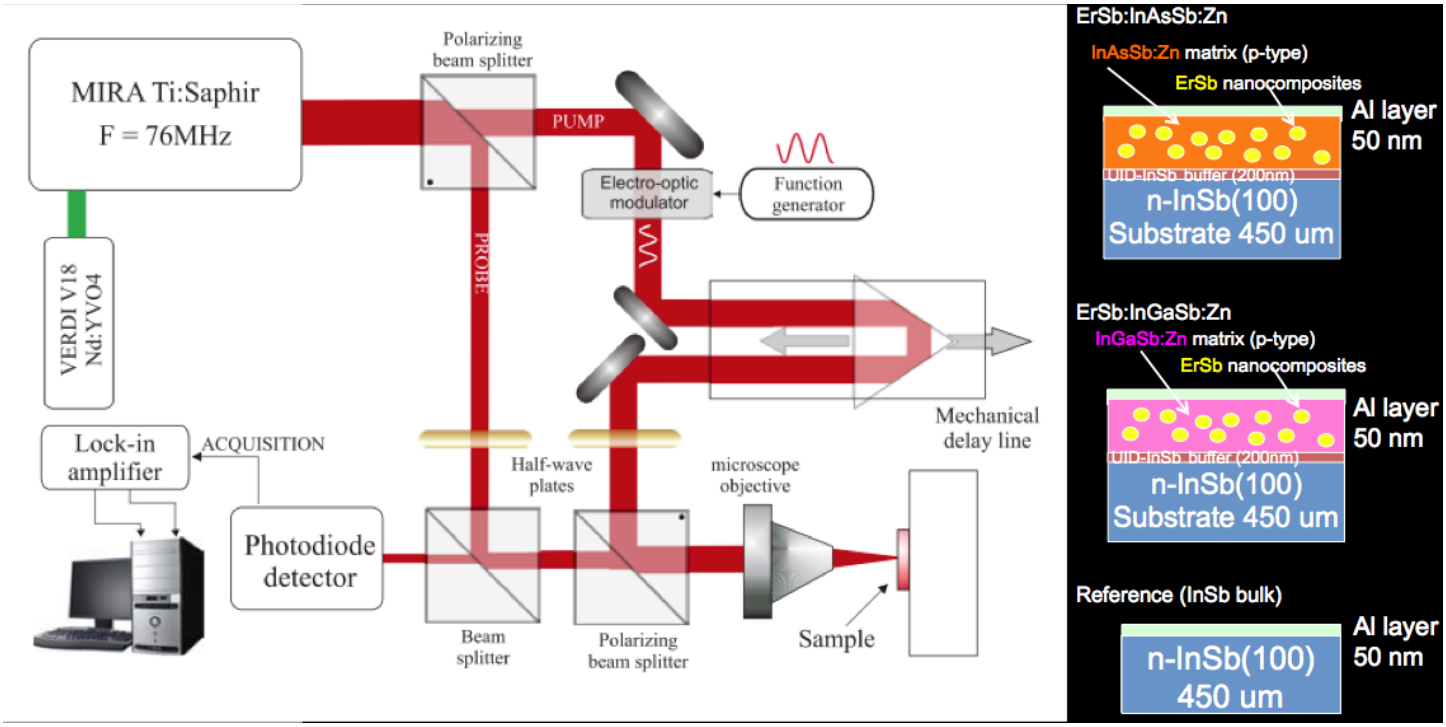

Figure 9 - Time Domain Thermo Reflectance configuration and required sample structures for thermal conductivity measurement of grown film on InSb(100) substrate.

3. Results (the analysis feels a little light and has information placement and flow problems but a good start)

3.1 The growth of InSb on InSb(100) substrate and characterization

The surface of InSb(100) substrate was thermally deoxidized before the epitaxy process started and the deposition was conducted for 2 to 3 minutes until InSb layers grow about 1.2 μm thickness on epi-ready substrate. The growth time was controlled in-situ interferometer technique of grown layer on quartz glass or Si substrate.

The electric properties and temperature dependency of Seebeck coefficient (thermoelectric power) and electrical conductivity were measured on the grown films.

The InSb layers had p type properties as expected. Seebeck coefficient increased first and had local maximum at 495 K then finally started monotonic drop in the high temperature region as the thermally excited electrons in the n type substrate dominated the carrier population. On the other hand, the electric conductivity monotonically decreased as the temperature rising because the scattering rate of carriers by excited phonons increased in the materials. (good info but could to increase writing and put between figures or it's a huge block of writing then a bunch of picture)

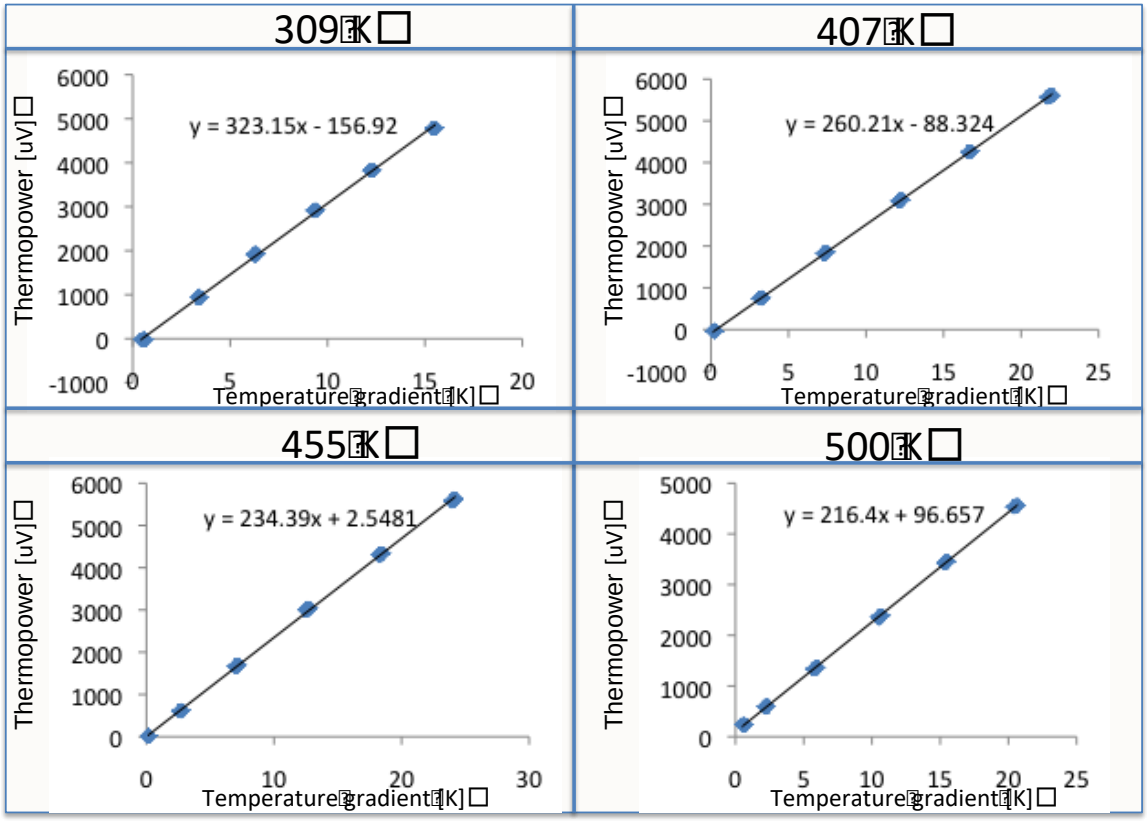

Figure 10 - Seebeck coefficient (thermoelectric power) of p type InSb grown film at four temperature steps. The thermoelectric power was measured against temperature gradient between hot and cold end of the sample chips in unit of Kelvin. The slope of each line indicated Seebeck at the temperature steps respectively.

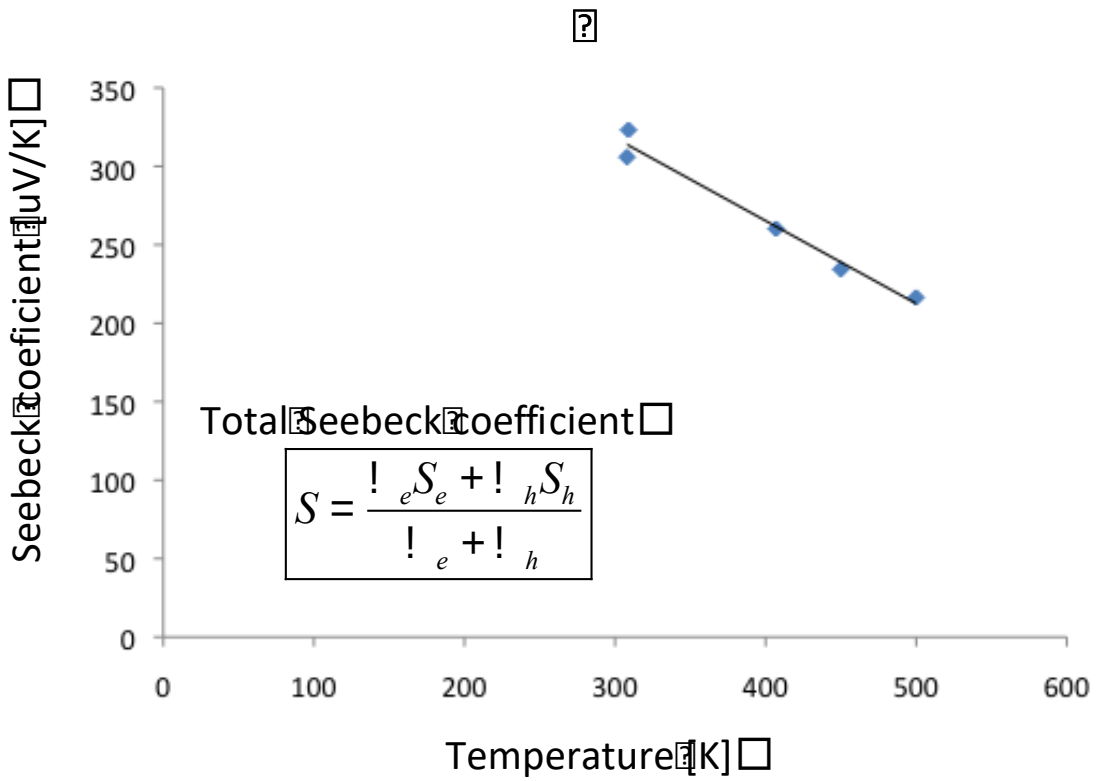

Figure 11 - The plot of Seebeck (thermoelectric power) coefficient slopes in Fig. 2. Since the thermoelectric power depends on the contribution of both electron and hole shown in the formula in the figure, Seebeck showed monotonic decrease against temperature rising. (Hiro's comment: top point at 300 K will be removed because the measurement was not conducted in the vacuum as well as the other points at higher temperature steps.)

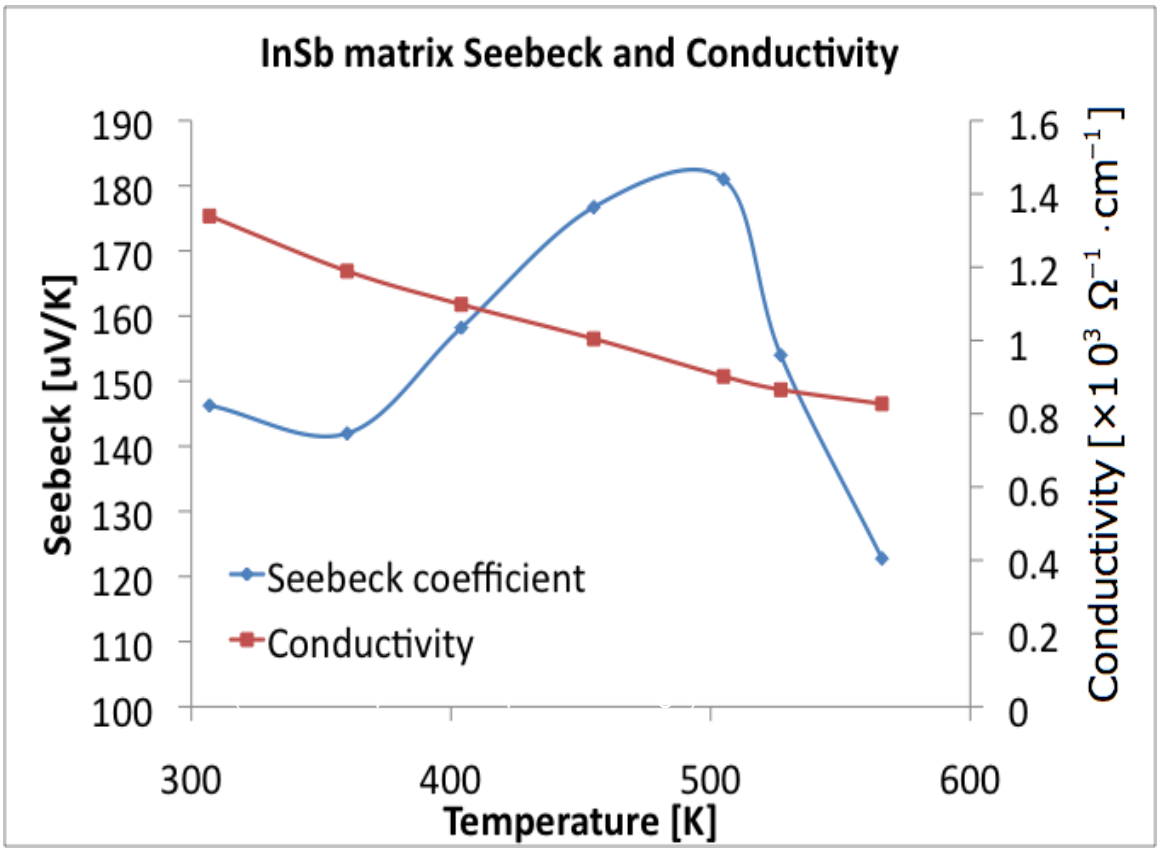

Figure 12 - Temperature dependency of Seebeck coefficient (blue curve) and electric conductivity(red curve) of InSb thin film grown on n type InSb(100) substrate. Seebeck coefficient increased first then started drop at 495 K as the n type substrate dominated the electric properties due to thermally excited electrons became majority carrier. The electric conductivity monotonically decreased as the temperature increased. Both properties showed the tendencies that were expected in p type semiconductors.

3.2 The growth of ErSb on InSb(100) substrate and characterization

The very first challenge of erbium mono antimonide thin film growth on Indium antimonide (100) substrate by MOCVD was successfully conducted. Seeking a good growth condition, we found the growth rate of ErSb thin film had strong sensitivity to the growth temperature and Er/Sb precursor flow rate ratio. The growth rate showed a sharp peak 47 Å/min. (angstrom/min) in the growth condition of substrate temperature at 485 °C and the precursor flow rate ratio 2.25 (Figure 13). The grown films at the maximum rate showed smooth morphology implying good crystal quality shown in (Figure 14) <here need SEM image of ErSb film on InSb(100) sub> and EDX scan identified all expected elements Er, Sb, and In (Figure 15). Also XRD spectrum of the grown ErSb layer on the InSb substrate indicated formation of two distinct single crystal, ErSb(422) and ErSb(511) (Fig.). However, the spectrum has not suggested any sign of ErSb(200) and ErSb(400) atomic layers in our ErSb epitaxy. (figure? At the end feels wierd)

3.3 Ex-situ erbium monitoring

We describe an ex-situ monitoring technique for a small amount (~30 mono-layers) of erbium monoantimonide (ErSb) deposited on an indium antimonide (InSb) epitaxial layer prepared on InSb (100) substrates by metal organic chemical vapor deposition (MOCVD). Our objective is to improve thermoelectrics properties of nanocomposites that employ nanometer size semi-metallic ErSb particles (ErSb nanoparticles) embedded in ternary group III-V compound semiconductor host materials such as indium gallium antimonide (InGaSb) and indium antimonide arsenide (InSbAs). The formation of ErSb nanoparticles embedded in a host material is spontaneous and needs to be carefully controlled to tune the size and volume density of the ErSb nanoparticles. We used an ex-situ monitoring technique based on glancing-angle infrared-absorption, reflection absorption infra-red spectroscopy (RAIRS), to study the formation of ErSb nanoparticles to correlate the amount of delivered ErSb and surface morphology of the surface of InSb covered with ErSb. (location?)

Figure 17 shows RAIRS spectrum collected from the four samples with various nominal ErSb coverage (7.2, 9.5, 14.3, and 21.5 ML) on hydrogen terminated InSb surfaces. As clearly seen, the absorption associated with the In-H bonds decreases as the amount of ErSb on the InSb surfaces increases. The smallest increment of 2.3 ML from 7.2 ML to 9.5 ML can be distinguished, which suggests that RAIRS is a capable ex-situ tool for calibrating a small amount of ErSb on InSb when the surface of InSb is saturated with hydrogen. The peaks correspond to those reported for In-H stretching modes [6] [7].

Figure 18 shows AFM images collected on two of the ErSb samples with ErSb 7.2 ML (left) and 21.5 ML (right).. The images clearly show that the surface of the InSb buffer layer is covered by a numerous ErSb islands with surface coverage of 65.3 % for the 7.2 ML ErSb sample and 81.5 % for the 21.5 ML ErSb sample., which is consistent with the RAIRS results that the incident infra-red is absorbed by In-H bonds present on the exposed InSb buffer layer partially covered by ErSb islands.

Based on the ErSb deposition rate 49 Å/min., Er flow rate ratio, and growth time 3 min, we converted the amount of segregated Er into the number of mono layer which is the number of deposited ErSb layer averaged over the substrate area. The Er precursor flow rates 6.0, 8.0, 12.0, and 18.0 E-6 mole/min are interpreted as 7.2, 9.5, 14.3, and 21.5 ML respectively. The more Er precursor flow rate per minute get increased, the less the RAIRS absorption got be. Besides, the absorption peaks aligned at 1755 cm^-1 well matched to In-H stretching mode in the literature [6] [7]. Hereby we concluded that the In-H stretching bonding on the InSb(100) was getting masked by grown ErSb grains then the absorption of IR was getting weaker as the segregated ErSb increased.

3.4 Co-deposition results of ErSb nanocomposite with zinc doped III-V host materials

Electro Chemical Voltage (ECV) measurement was conducted on four different zinc dose amount layers separated 50 nm UID InSb barrier layers grown on 200nm UID InSb buffer layer prepared on n type InSb(100) substrate (Figure 17). Although the ECV curve revealed doped Zn diffused through the barrier layers and showed smoothed carrier density from top layer to substrate, small steps at arrows were still recognizable and provided the capability of carrier tuning in zinc dose amount range (1.7 – 2.05 E+20, 1.1 – 1.4 E+20, 6.4 – 9.2 E+19, and 4.03 – 6.02 E+19 cm^-3) from the top layer (sample surface) to bottom layer (substrate).

XRD spectrum in InGa_xSb_1-x:Zn (X=0.975) (Figure 18) and In_1-yAs_ySb:Zn (Y=0.406) (Figure 19) indicated full range and about half range of ternary alloy component tuning respectively.

TEM cross section imaging indicate uniformly distributed 20 ~ 35 nm diameter ErSb nanocolum grown vertically in InGaSb:Zn host material (Figure 20) and uniformly distributed 20 ~ 30 nm diameter ErSb nanoparticles in InAsSb:Zn host material (Figure 21) in the grown samples. Where TEM image in Fig. 11 and 12 are taken with electron acceleration voltage at 200 kV. The sample lamellas are processed by Ga iron beam FIB acceleration voltage at 30 kV using vertical curving technique. (1) The processed area is covered by Pt barrier layer, (2) 4 um depth vertical trenches are created in the both side of the lamella, (3) The underneath cut and the left and right slits are created, (4) The both surface of the lamella are polished by the iron beam into 50 ~ 60 nm thickness, (5) The lamella is scraped off and transferred by tipped glass capillary micro-manipulator onto a copper TEM grid. (hmmm what figure are you referring to here? I would say figure I which would belong in a different section not results)

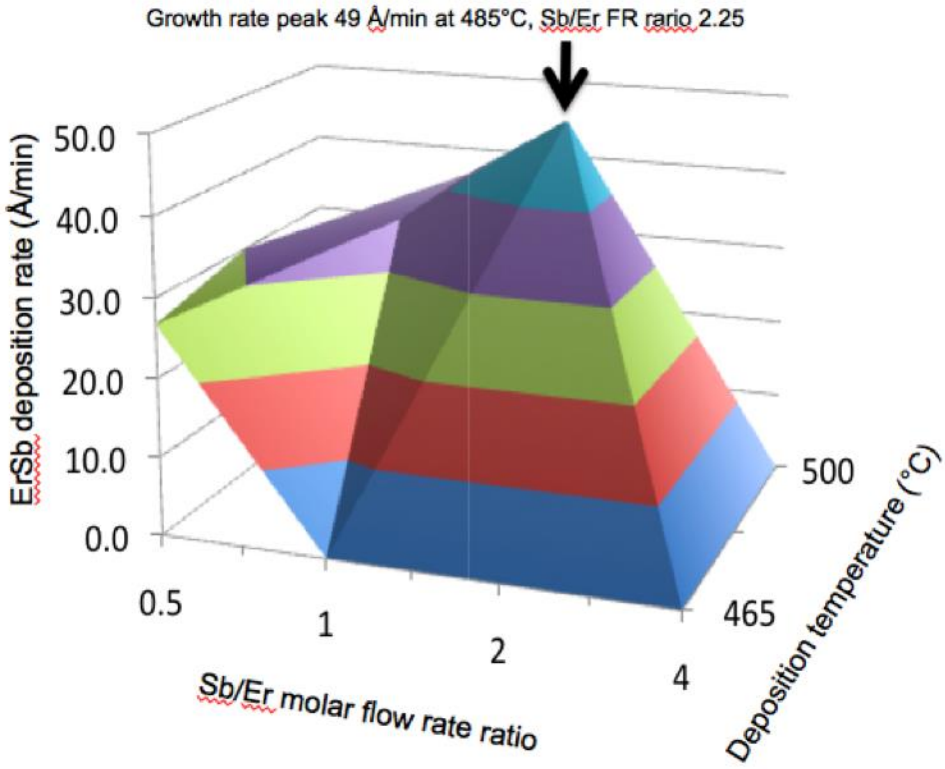

Figure 13 - ErSb deposition rate on InSb (100) substrate has strong sensitivity to the deposition temperature and the Sb/Er precursor flow rate ratio. The peak deposition rate 49 Å/min was obtained at 485 °C and the Sr/Er flow rate ratio of 2.25.

(um where is fig 14?)

Figure 14 – SEM image of ErSb film grown on InSb(100) substrate. The surface had smooth morphology indicating formation of single crystal.

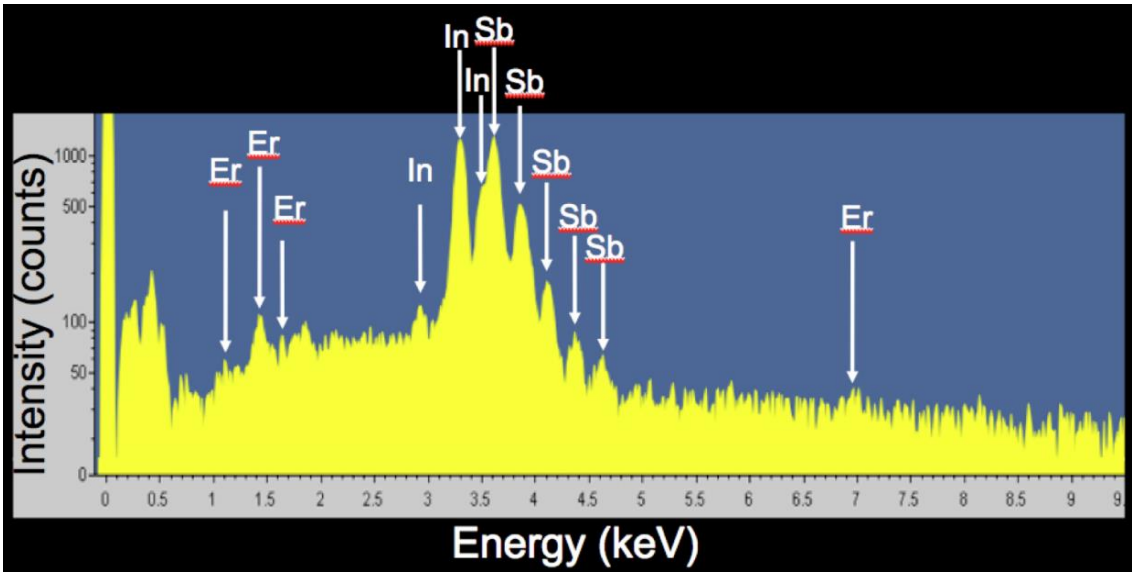

Figure 15 - EDX spectra of Er deposition samples on InSb(100) substrate. All component elements in the grown film and substrate appeared in the spectrum.

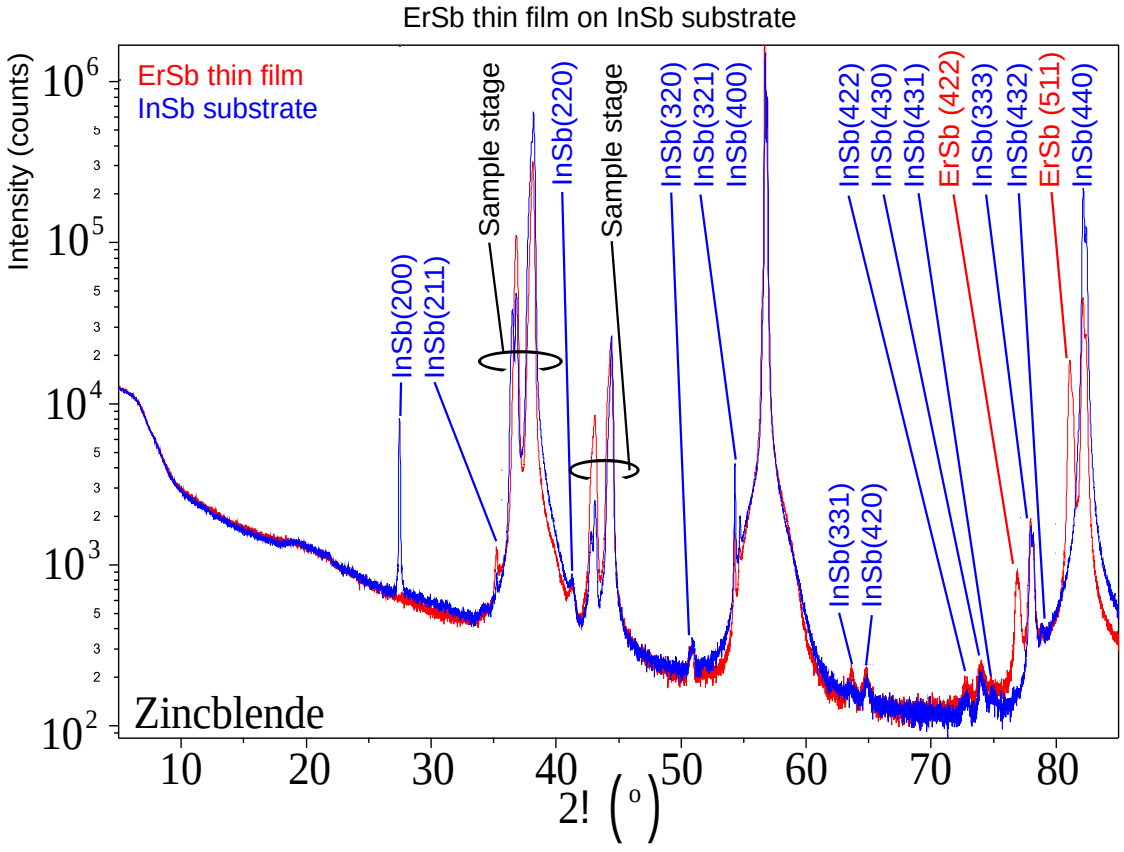

Figure 16 - XRD spectra of ErSb thin film. The spectra on ErSb film indicates ErSb single crystal structure showing ErSb (422) and ErSb (511) peaks.

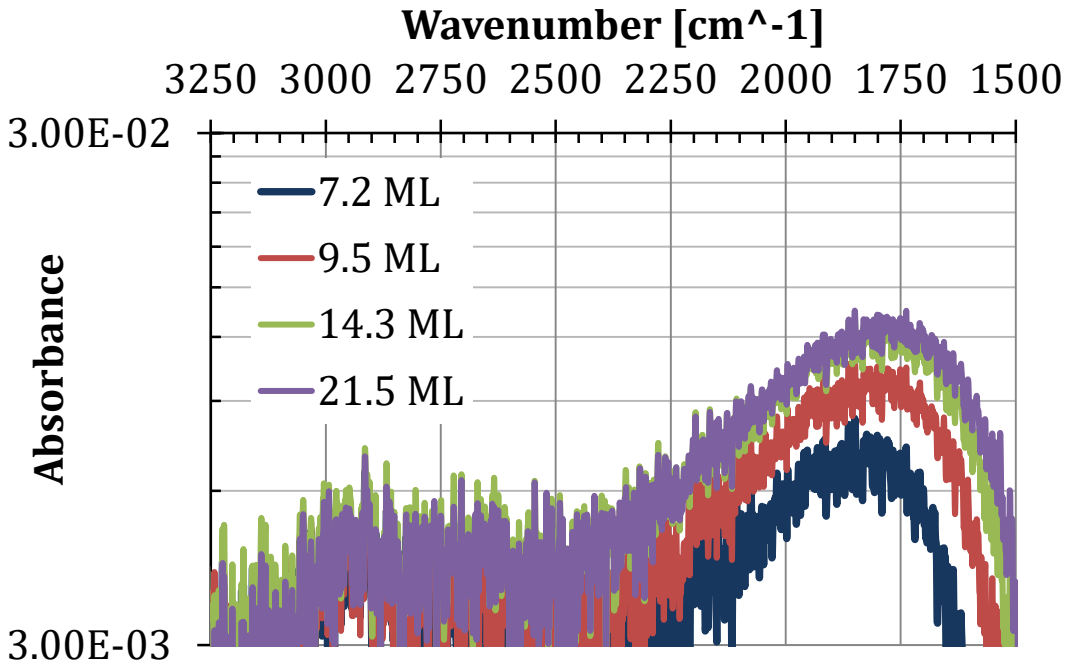

Figure 17 - RAIRS spectra collected from the four ErSb samples with various total ErSb coverage (7.2-21.5 ML) on hydrogen terminated InSb surfaces.

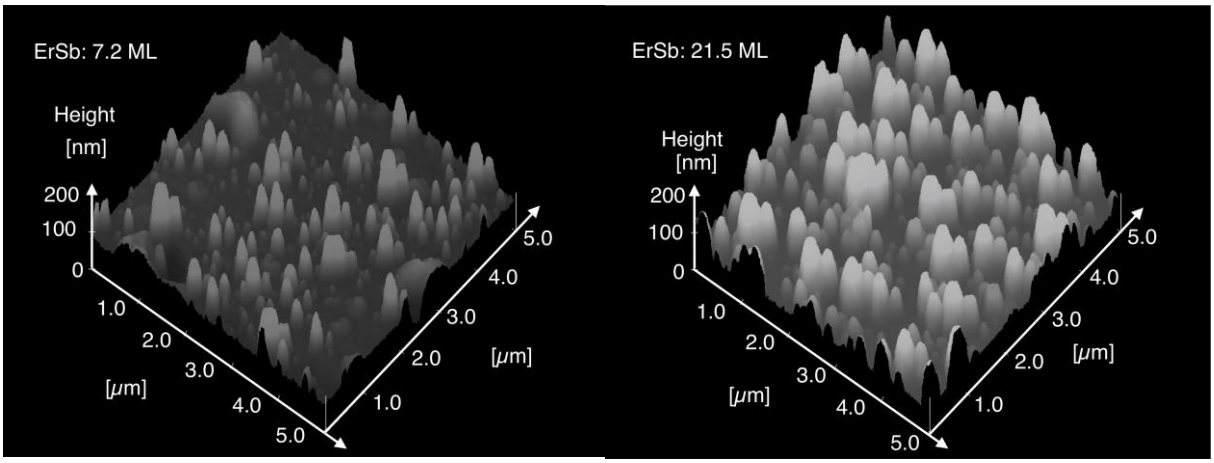

Figure 18 - AFM images of two distinctive ErSb coverage on the surface of InSb buffer layer. The 65.3 % of 7.2 ML sample surface was covered by grown ErSb (left) while 81.5 % surface was covered by ErSb in 21.1 ML sample (right).

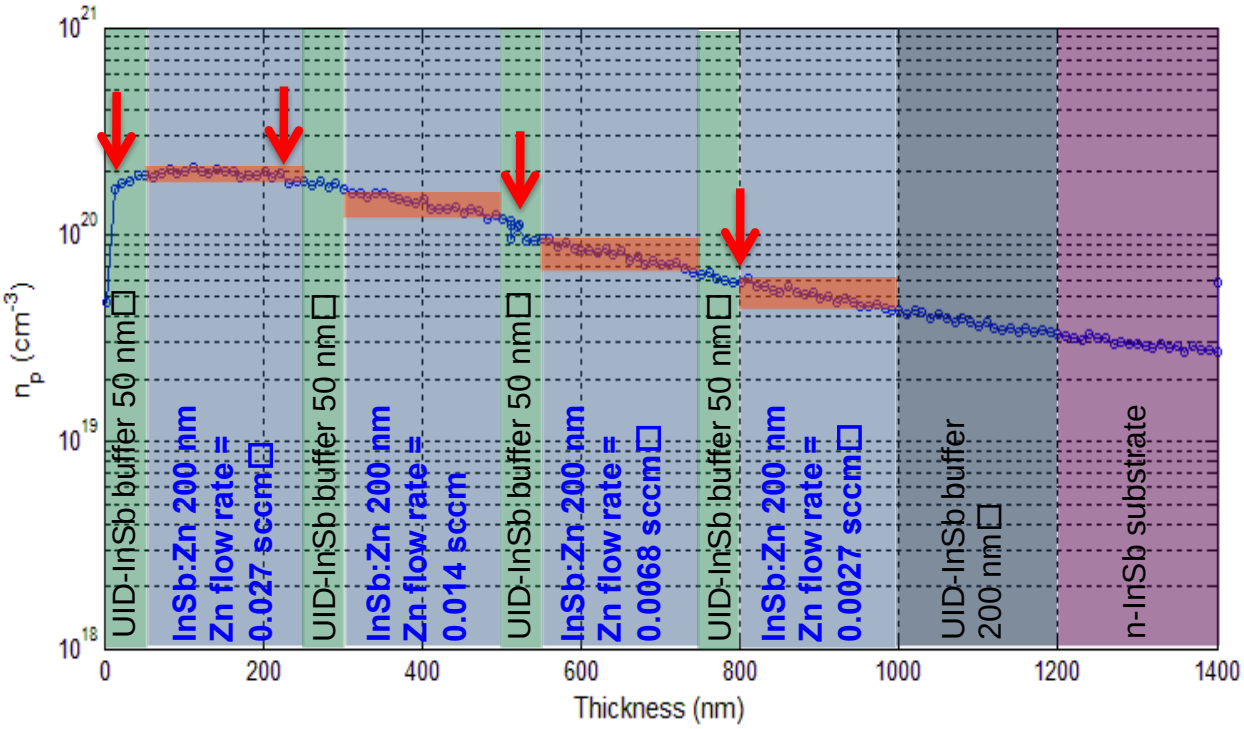

Figure 19 – Electro Chemical Voltage (ECV) measurement result on four various Zn dose amounts (12.2 E+7, 6.12 E+7, 3.04 E+7, and 1.21 E+7 cm^-3) in InSb layers. From top to bottom, Zn doped InSb layers were grown with Zn precursor flow rate 0.027, 0.014, 0.0068, and 0.0027 sccm respectively. The carried density curve showed smooth feature with due to Zn diffusion getting through all UID InSb separation layers (50 nm thickness) and UID InSb buffer layer (200 nm thickness).

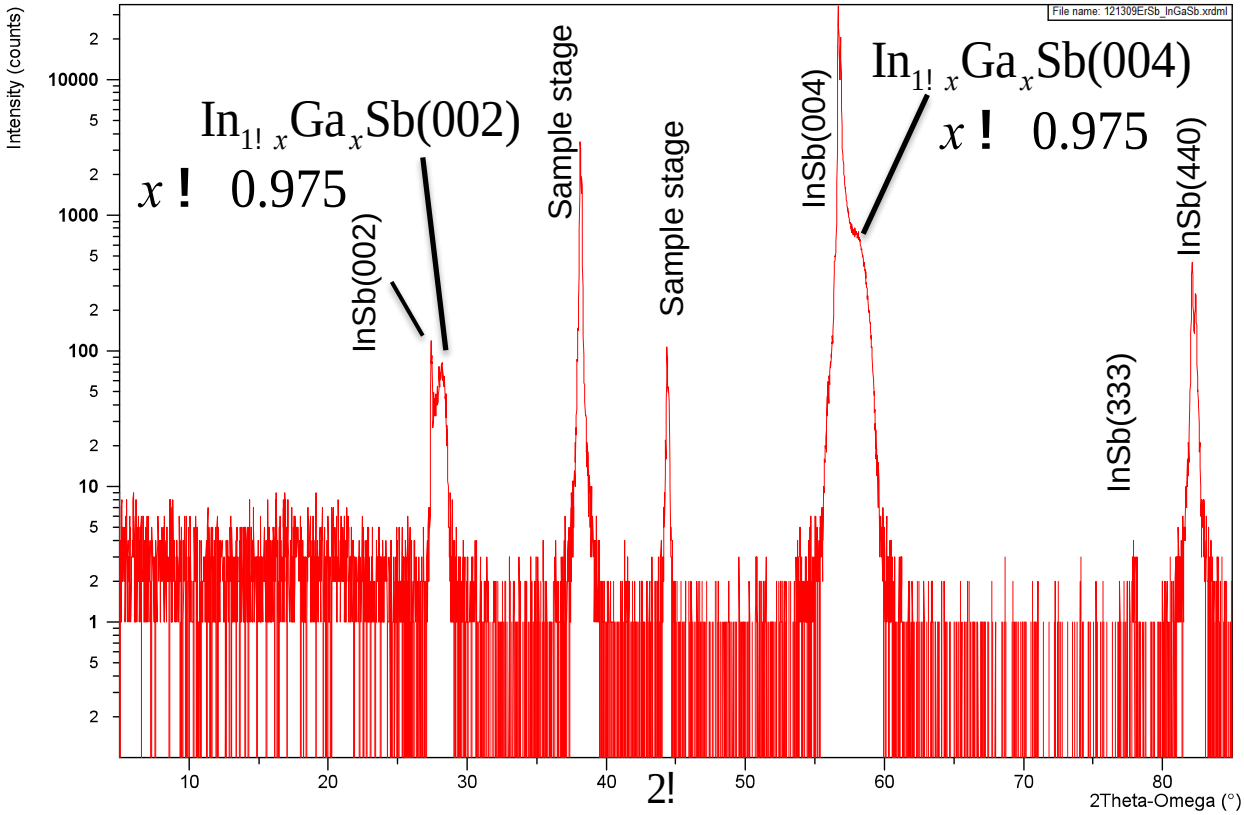

Figure 20 – XRD peak shift of In_1-xGa_xSb:Zn (X=0.976)

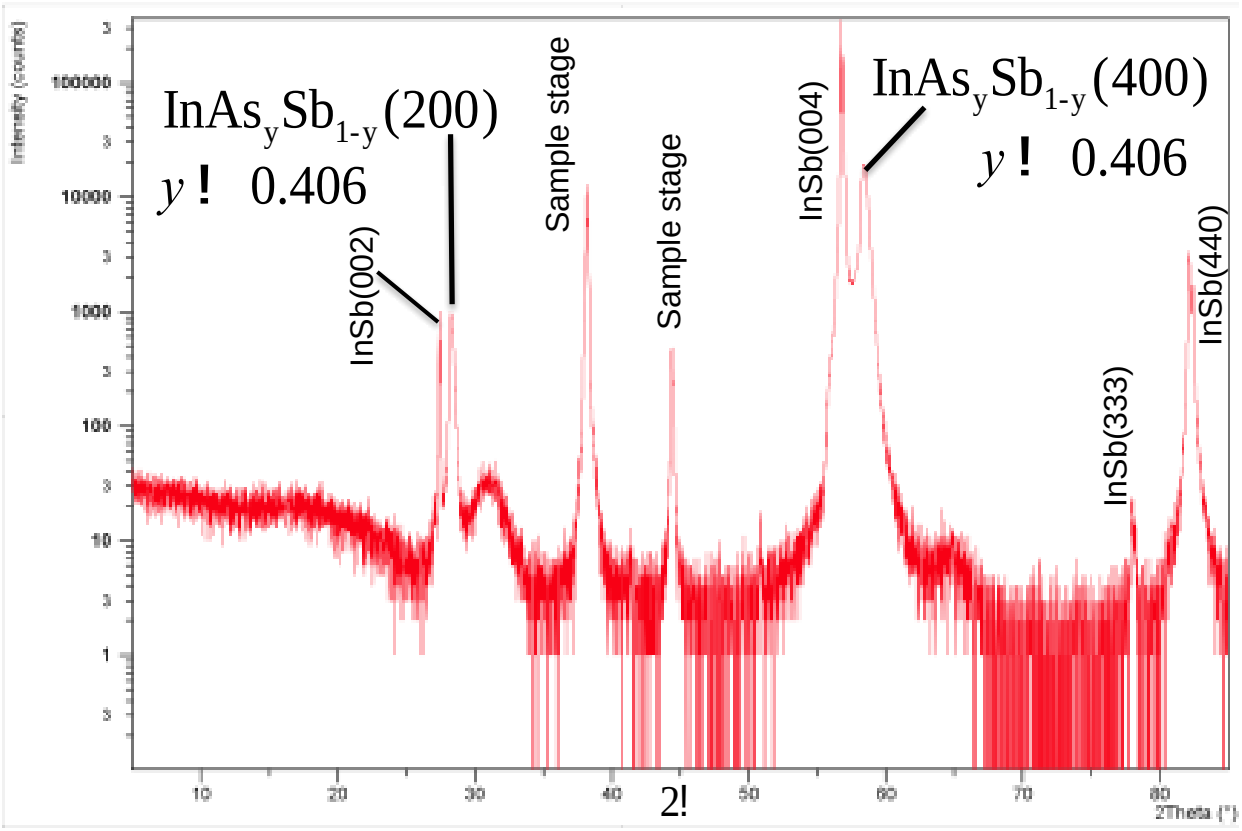

Figure 21 – XRD peak shift of InAs_ySb_1-y:Zn (Y=0.406)

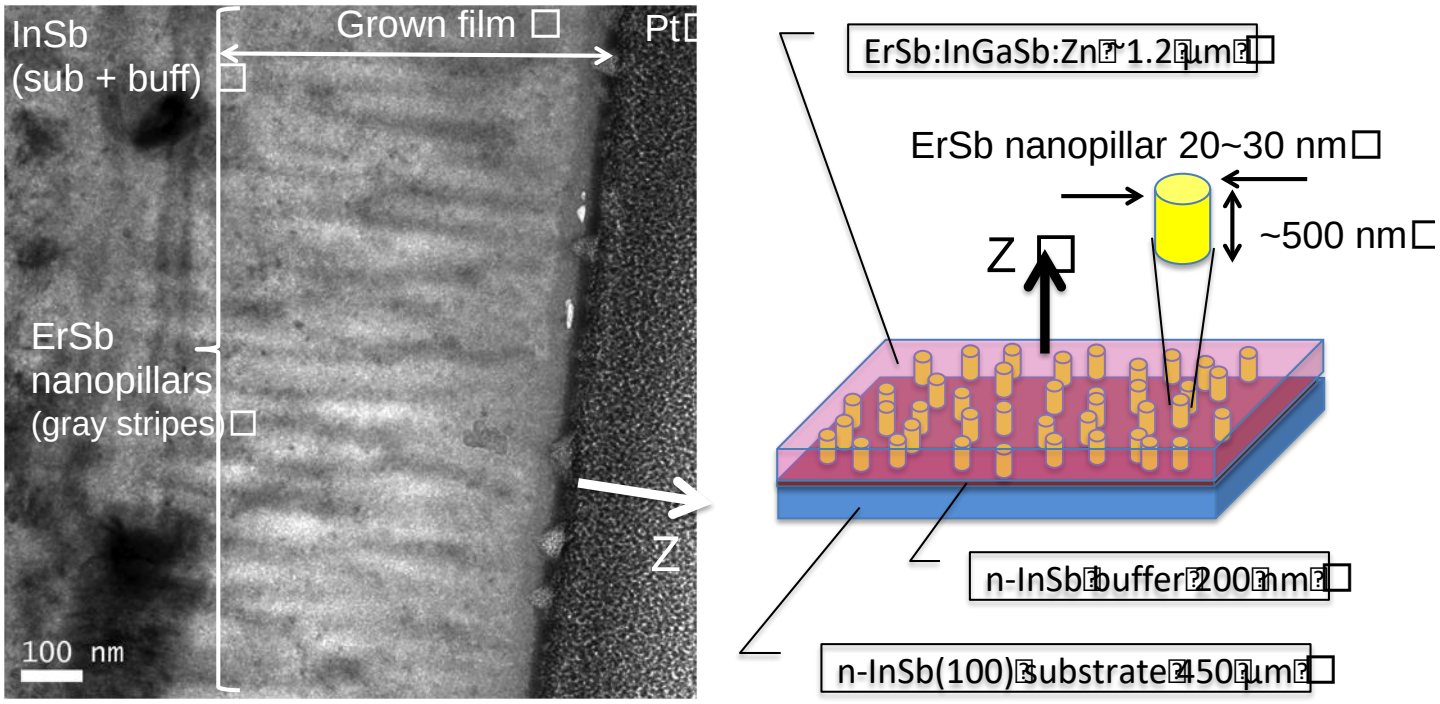

Figure 22 – TEM image of InGaSb:ErSb shows uniformly distributed 20 ~ 35 nm diameter nanocolumn in InGaAs:Zn matrix layer.

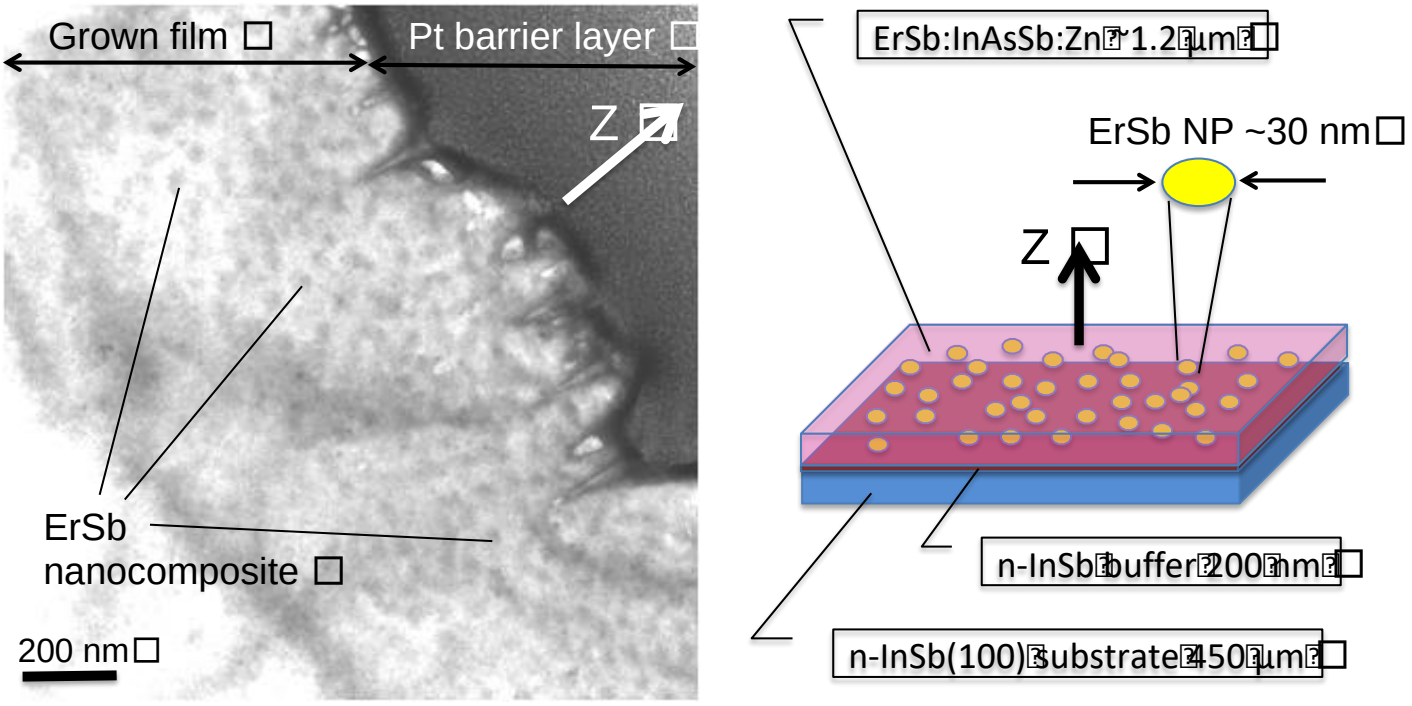

Figure 23 – TEM image of InAsSb:ErSb shows uniformly distributed 20 ~ 35 nm diameter nanoparticles in InGaAs:Zn matrix layer. E-beam went into the sample from [110] directions respectively.

Discussion

In terms of carrier tuning, zinc was doped in the host materials. However, Zn has quite high diffusivity in the grown film then it have made samples have resistive electric characteristics combined with n type InSb(100) substrate. The ECV curve indicated Zn spread through not only 50 nm thickness UID InSb buffer (barrier) layer and but also the 200 nm thickness UID InSb buffer layer. The ECV measurement result showed entire multilayer samples separated with UID InSb buffer layers had resistive electric characteristics between the front and back side of the sample chips. Along with small band gap of the host material InSb (Eg = 0.17 eV), it has been hard to separate the influence of substrate's electric properties from ones of the grown film. Then we concluded the host material change from InSb to relative to larger band gap materials i.e. InP (Eg = 1.? eV)

The grown ErSb films and grains on InSb(100) substrate and UID InSb buffer layer prepared on InSb(100) substrate have not shown ErSb(200) and ErSb(400) peaks while ErSb(422) and ErSb(511) peaks were maintained in the XRD spectrum. This phenomena indicated an unconventional extinction mechanism was working in the grown film holding mono crystal structures. Palmstrøm reported rare earth – group V rock salt crystal growth on zinc blende substrate [2], [3]. They suggested the grown crystal had the rotated orientation against the substrate crystal structures.(connection please)

Conclusion (wrap it up and why do I care?)

We successfully demonstrated p type ErSb nanocomposites co-deposition with two Zn doped ternary host materials InGa_xSb_1-x:Zn and In_1-yAs_ySb:Zn by MOCVD. The full rage of Sb substitution with Ga and half ratio of In substitution with As were confirmed by XRD peak shifts. In

InGaSb:Zn matrix, ErSb aggregated as uniformly distributed nanopillars vertical to substrate surface with 500 nm in the length and diameter up to 35 nm while uniformly distributed ErSb nanoparticles with diameter of 20 to 50 nm in the InAsSb:Zn matrix. Then TDTR thermal conductivity measurement results in showed good agreement with those of simulation results of ternary alloys. That indicated that ErSb nanoparticles (deamete 20 to 30 nm) co-deposited InAsSb:Zn host ternary alloy could show further thermal conductivity reduction (4.0 ± 0.6 W/m·K) beyond the alloy limit of InAsSb (4.0 W/m·K). That implied that realization of improvement of dimensionless figure of merit $ZT = S^2 \sigma T / (k_{lattice} + k_{carrier})$ through decrease in lattice thermal conductivity $k_{lattice}$.
The very first ErSb growth by MOCVD was conducted on InSb(100) substrate. The grown ErSb indicated two different single crystal formation ErSb(422) and (511) but no indication of (200) atomic plane showing smooth surface morphology and expected component elements in the film.
Along with ErSb growth and nanocomposite co-deposition with host materials by MOCVD, we developed ex-situ small amount Er monitoring technique employing RAIRS. That allows us to sense the variation of deposited ErSb in the increment of 2.3 ML (2.0 E-6 mole/min.) detecting IR absorption intensity change by In-H stretching bond on InSb(100) substrate surface. The original InSb substrate surface masked by porous ErSb films deposited.
We conclude here that MOCVD growth of ErSb nanocomposites co-deposition with zinc doped InSb base host materials was established and the thermoelectrics property of grown films could achieve or beyond that of the base materials.
MOCVD samples with nanocomposites embedded thermoelectric host materials showed comparable thermoelectric properties as that of MBE samples. We could cover wide range of sample parameters, scale up of experiment because MOCVD has high growth rate and easy to scale up.

Acknowledgment

Prof. Nobby Kobayashi, Prof. Ali Shakouri,

Elane Coleman, Dr. Gary Tompa of SMI. Inc.

Tela Favaloro,

Dr. Gilles Pernot, Stephan Kraemer, Dr. Hong Lu, Prof Art Gossard, Xiang Liu, Prof. Palmstrøm

References

[1]
G. Chen and M. S. Dresselhaus, et al., Int. Mat. Rev. 48 (1) pp 1 (2003).
G. Mahan, B. Sale et al., Phys. Today, Mar. pp 42 (1997).

J. M. Zide et al., Appl. Phys. Lett., vol. 87 (11) pp. 112102 (2005).

[2]
I. Terasaki et al., Phys. Rev. B, vol. 56 (20) pp.165127, (1997).

[3]
C. J. Palmstrom, Annu. Rev. Mater. Sci., vol. 25, pp. 389 (1995).

[4]
C. Palmstrom, T. Sands, J. Harbison, and et al, Proceedings of SPIE Vol.1285 Growth of Semiconductor Structures and High-Ta Thin Films on Semiconducotrs. (1990).

[5]
I. J. V. D. PAUW, Philips Research Report, vol. 13 (1) pp.1 (1958).

[6]
P. Pullumbi, et al., Chemical Physics, vol. 185, pp. 25 (1994).

[7]
K. Raghavachari et al., Journal of the American Chemical Society, vol. 124, (50), pp. 15119, (2002).

[8]